Dynamic evolution of tidal networks under the combined effect of de-reclamation and decrease of sediment supply

Yu, Shang; Xu, Fan; Peng, Zhong; Guo, Leicheng; Wang, Xianye; Xie, Weiming; Zhu, Chunyan; Wang, Zhengbing; He, Qing

DOI
10.1016/j.csr.2024.105274

Publication date
2024

Document Version
Final published version

Published in
Continental Shelf Research

Citation (APA)
Yu, S., Xu, F., Peng, Z., Guo, L., Wang, X., Xie, W., Zhu, C., Wang, Z., & He, Q. (2024). Dynamic evolution of tidal networks under the combined effect of de-reclamation and decrease of sediment supply. *Continental Shelf Research*, *279*, Article 105274. https://doi.org/10.1016/j.csr.2024.105274

Continental Shelf Research 279 (2024) 105274

Contents lists available at ScienceDirect

Continental Shelf Research

journal homepage: www.elsevier.com/locate/csr

Dynamic evolution of tidal networks under the combined effect of de-reclamation and decrease of sediment supply

Shang Yu [a], Fan Xu [a,*], Zhong Peng [a], Leicheng Guo [a], Xianye Wang [a], Weiming Xie [a], Chunyan Zhu [a], Zhengbing Wang [b,c], Qing He [a]

[a] State Key Laboratory of Estuarine and Coastal Research, East China Normal University, Shanghai, 200241, China
[b] Faculty of Civil Engineering and Geosciences, Section of Hydraulic Engineering, Delft University of Technology, Stevinweg 1, 2628 CN, P.O. Box 5048, 2600 GA, Delft, the Netherlands
[c] Deltares, Rotterdamseweg 185, P.O. Box 177, 2600 MH, Delft, the Netherlands

ARTICLE INFO

Keywords:
Tidal networks
Morphodynamic modeling
de-reclamation

ABSTRACT

De-reclamation is a common strategy used for the restoration of tidal flats. In this study, we investigate the morphodynamic response of tidal channel networks and tidal flats after de-reclamation initiatives using the Delft3D numerical model. We find that tidal channel networks that have undergone reclamation and retreat projects have a lower drainage density (8.95 km^{-1}) than that of channel networks that formed naturally (11.33 km^{-1}), and the drainage efficiency of natural formed channel networks is almost three times greater than restored channel networks. These findings indicate that de-reclamation alone cannot fully erase the imprinting of the previous reclamation. We also find that the ultimate effectiveness of de-reclamation is affected by the geographical layout and unchanneled path length of the inchoate main creek system. In addition, following the implementation of de-reclamation, the immediate opening of previously enclosed areas amplifies the tidal prism, thereby intensifying tidal scouring and resulting in significant erosion, with erosion rate reaching hundreds of millimeters per day. Such losses can be remediated under sufficient sediment supply and prevented through the construction of artificial channels. However, this severe erosion may escalate under an insufficient sediment supply or a heightened tidal prism, potentially leading to permanent loss. These findings constitute an important reference for future engineering practices that support the safety and sustainability of coastal resources.

1. Introduction

The global extent of tidal flats is shrinking annually by approximately 1–2% (Adam, 2002; Duarte et al., 2008). This shrinkage is largely driven by reclamation activities (Gu et al., 2018; Murray et al., 2019). Each year, reclamation projects claim over 8000 km^2 of these critical ecosystems (Pendleton et al., 2012; Zhong and Hu, 2021). This area loss has precipitated a multitude of environmental challenges, including the degradation of coastal habitats, decline in biodiversity, and increased risk of coastal flooding (Choi et al., 2014; Choi, 2019; Lee et al., 2018; Yang et al., 2011; Zhang et al., 2018). These adverse impacts have motivated various strategies for ecosystem recovery, aiming at reducing human impacts, reviving ecosystems, and constructing new habitats (Aronson and Le Floc'H, 1996; Aronson et al., 1993; Cairns and Heckman, 1996).

De-reclamation is a common strategy used for the restoration of tidal flats (Yang et al., 2010; Susanne and Robert, 2007). After removing embankments (Fig. 1), natural processes reclaim the enclosed area, often triggering significant feedbacks. Various embankment removal methods exist, including creating small openings and performing total removal. These different approaches inevitably precipitate distinct geomorphic responses, including the redistribution of flow and sediment, vegetation colonization, and establishment of new ecosystems (Cadier et al., 2020; Liu et al., 2021; Ren et al., 2011; Williams et al., 2002; Wolters et al., 2005). Given this complexity, it is crucial to carefully evaluate the outcomes of embankment removal (French, 1999; Wolters et al., 2005; Katwijk et al., 2016; Mumby and Steneck, 2008).

A prominent morphological change following de-reclamation is the expansion of tidal networks, which act as pivotal conduits for material and energy exchange between the intertidal zone and neighboring waterbodies (Desroy and Denis, 2004; Fagherazzi et al., 1999; Leonard et al., 1995; Rauch and Denis, 2008; Xie et al., 2018). The intricate

* Corresponding author.
E-mail address: fxu@sklec.ecnu.edu.cn (F. Xu).

https://doi.org/10.1016/j.csr.2024.105274
Received 11 October 2022; Received in revised form 26 May 2024; Accepted 1 July 2024
Available online 5 July 2024

geometry of these networks has been identified as a vital metric for estimating the current state and projecting future trends of tidal flats (Jarzemsky et al., 2013; Liu et al., 2021; Simenstad et al., 2006; Takekawa et al., 2010). Tidal flow is the driving factor of tidal channel network development (Coco et al., 2013; Guo et al., 2015; D'Alpaos et al., 2007; Marani et al., 2002). The spatial patterns of tidal networks are also controlled by details of the tidal basin geometry, like.g., sand barrier extinction, lagoon terrain, and river position (Goudie, 2013; Marani et al., 2003; Zhou et al., 2014a). Although extensive research has focused on the bio-morphodynamics of tidal networks in recent decades, specific scenarios of de-reclamation remain underexplored. Chen et al. (2020) made a seminal attempt to address this gap by employing numerical models to elucidate the centennial-scale morphological evolution. However, field observations have revealed that morphological changes after de-reclamation occur on much shorter timescales (Anisfeld et al., 2016; Takekawa et al., 2010). The effects of different hydrodynamic, landscape, and artificial conditions (e.g., tidal range, slope, and demolition schemes) on the results of de-reclamation have not been thoroughly studied.

In this study, we employ the state-of-the-art numerical model Delft3D to investigate the morphodynamic evolution of tidal networks in the wake of de-reclamation activities—particularly under conditions of sediment supply reduction. Specifically, we aim to answer the following questions: (1) To what extent can topography revert to its natural state following de-reclamation? (2) What are the characteristic geomorphic changes that correspond to different de-reclamation strategies? (3) How does the decline in sediment supply influence the evolution of tidal networks after de-reclamation? By tackling these research questions, this study provides valuable insights that could inform subsequent engineering interventions and contribute to the sustainable management of coastal resources.

2. Methods

2.1. Model description

The Delft3D numerical model comprises modules for hydrodynamics, sediment transport, and morphodynamic evolution (Fagherazzi et al., 2012; Lesser et al., 2004; van der Wegen and Roelvink, 2008, 2012). In this study, the model executes a cyclical iterative procedure: (1) It calculates the tidal flow field based on the 2D shallow water equations; (2) it estimates the suspended sediment transport through the advection–diffusion equation; and (3) it predicts morphological changes based on the bed continuity equation. This modeling approach has been successfully employed to simulate the morphodynamic evolution of tidal creek networks (Chen et al., 2020; Wang et al., 2019; Xu et al., 2017; Zhou et al., 2014a; Zhou et al., 2021). The fundamental equations are as follows.

Two-dimensional shallow water equations.

$$\frac{\partial \eta}{\partial t}+\frac{\partial (d+\eta)u}{\partial x}+\frac{\partial (d+\eta)v}{\partial y}=0, \tag{1}$$

$$\frac{\partial u}{\partial t}+u\frac{\partial u}{\partial x}+v\frac{\partial u}{\partial y}=-g\frac{\partial \eta}{\partial x}-g\frac{u\sqrt{u^2+v^2}}{C^2(d+\eta)}+\nu_w\left(\frac{\partial^2 u}{\partial x^2}+\frac{\partial^2 u}{\partial y^2}\right), \tag{2}$$

$$\frac{\partial v}{\partial t}+u\frac{\partial v}{\partial x}+v\frac{\partial v}{\partial y}=-g\frac{\partial \eta}{\partial y}-g\frac{v\sqrt{u^2+v^2}}{C^2(d+\eta)}+\nu_w\left(\frac{\partial^2 v}{\partial x^2}+\frac{\partial^2 v}{\partial y^2}\right), \tag{3}$$

where t is time (s); x and y are the Cartesian coordinates (m); d is the still water depth (m); η is the tidal level (m); u and v are the depth-averaged velocities components (m/s); g is gravity (m/s^2); C is the Chézy friction coefficient (m$^{1/2}$/s); and ν_w is the eddy viscosity (m^2/s).

The Chézy coefficient is calculated as follows:

$$C=\frac{d^{1/6}}{n}, \tag{4}$$

where n is the Manning coefficient equal to 0.025 s/m$^{1/3}$.

Advection–diffusion equation of suspended sediment transport.

$$\frac{\partial c}{\partial t}+\frac{\partial uc}{\partial x}+\frac{\partial vc}{\partial y}-\frac{\partial}{\partial x}\left(\varepsilon_{sx}\frac{\partial c}{\partial x}\right)-\frac{\partial}{\partial y}\left(\varepsilon_{sy}\frac{\partial c}{\partial y}\right)=0, \tag{5}$$

where c is the concentration of sediment (kg/m^3); and ε_{sx} and ε_{sy} are the eddy diffusivities of sediment (m^2/s).

Bed continuity equation.

$$(1-\varphi)\frac{\partial z_b}{\partial t}+\frac{\partial S_x}{\partial x}+\frac{\partial S_y}{\partial y}=0, \tag{6}$$

Fig. 1. Aerial view of a de-reclamation project in Jiangsu, China. (a) Reclaimed coastal area, photographed in February 2017 and (b) restored tidal flats after a de-reclamation project, photographed in September 2020. The latitude and longitude of the center of the presented area are 32° 56′ 06'' N and 120° 54′ 38'' E, respectively.

where z_b is the bed surface elevation (m); ϕ is the bed porosity (default 0.4; dimensionless); and S_x and S_y are the sediment flux components (m^2/s). The model can easily run in 2DH mode to simulate tides and sediment transport (Hu et al., 2009; Lesser et al., 2004). The grain size of the cohesive sediment in this study is less than 32 μm with a settling velocity (w_s) of 0.5 mm s^{-1} (Wiberg et al., 2015). The critical bed shear stress for erosion (τ_e) is set to 0.15 N/m^2. The sediment density is 2650 kg/m^3.

2.2. Model settings

We consider a 2500 × 5000 m rectangular computational domain, which is principally inspired by the de-reclamation project along the coast of Jiangsu, China (Fig. 1). The domain is discretized into 20 × 20 m cells. The bottom boundary experiences semidiurnal harmonic tides (cf. Chen et al., 2020; Zhou et al., 2014b), while the remaining three boundaries are closed. We experimented by applying Neumann boundary on the two lateral boundaries; however, the results were not significantly different (see supplemantary information for more details). The initial bathymetry features a gentle slope from land to sea, supplemented with minor perturbations to accelerate the onset of morphological adjustments (Zhang et al., 2018). The initial bed elevation conforms to Gaussian distributions, with 90% of elevation values falling between −15 and + 15 cm (Marciano, 2005).

Our comprehensive array of numerical experiments is listed in Table 1. Scenario N1 functions as a control case devoid of anthropogenic interventions, and all other scenarios undergo cycles of reclamation and subsequent de-reclamation processes. Initially, a thin dam isolates a cross-shore segment of 3000 m (measured from the seaward boundary) and divides the domain into 'reclamation area' and 'outer area' (Fig. 2f). Following a five-year model run to establish a relatively stable topography, we remove these barriers and simulate the ensuing morphodynamic adjustments following the de-reclamation projects. In scenarios C1–C4, we uphold a consistent sediment supply throughout the simulation period, albeit with varying boundary sediment concentrations. Conversely, scenarios D1–D4 involve a gradual reduction in sediment supply commencing after the fifth year, with different rates of decline. Moreover, scenarios B1–B4, T1–T4, and S1–S4 delve into the impacts of various factors, i.e., the moth in the reclamation dam, tidal amplitude, and initial bed slope of reclamation area, respectively. Furthermore, scenarios P1 and R1 are specifically devised to assess the consequences of previously incorporated artificial channels (morphological characteristics when de-reclamation occurs in scenarios P1 and R1 are in supplemantary information). Finally, scenario W1 is characterized by the demolition of embankments in two stages.

Table 1
Suspended sediment concentration (SSC) change and anthropogenic interventions in different scenarios.

Scenario	Specific settings
N1	SSC = 0.10 kg/m^3
C1	SSC = 0.10 kg/m^3
C2	SSC = 0.01 kg/m^3
C3	SSC = 0.05 kg/m^3
C4	SSC = 0.25 kg/m^3
D1	SSC decrease from 0.10 to 0.00 kg/m^3
D2	SSC decrease from 0.25 to 0.00 kg/m^3
D3	SSC decrease from 0.30 to 0.20 kg/m^3
D4	SSC decrease from 0.30 to 0.05 kg/m^3
D5	SSC decrease from 0.20 to 0.10 kg/m^3
B1	Mouth length = 500 m
B2	Mouth length = 900 m
B3	Mouth length = 900 m; mouth on the right
B4	Mouth length = 1300 m
P1	De-reclamation on deeper developed tidal channel networks
R1	De-reclamation on lower developed tidal channel networks
T1	Tidal amplitude = 0.50 m
T2	Tidal amplitude = 0.75 m
T3	Tidal amplitude = 1.25 m
T4	Tidal amplitude = 1.50 m
S1	Slope of reclamation area = 0.05%
S2	Slope of reclamation area = 0.075%
S3	Slope of reclamation area = 0.10%
W1	Demolish 500 m in the 5th year and demolish all in the 10th year

2.3. Morphometric analysis of network geometries

We employ a local adaptive threshold method to automatically discern the tidal network patterns from the simulated digital elevation model (DEM) data (Saxena, 2019; Uchida, 2013) and then extract the central lines of the channels using a thinning algorithm (Chen and Hsu, 1988). For the quantitative assessment of network geometries, we focus on the (1) drainage density, defined as the ratio of the total channel length to the drainage area (Stefanon et al., 2012); (2) unchanneled path length (Marani et al., 2003), approximated as the distance from a point on the flat to the nearest channel central line (Liu et al., 2021); and (3) drainage efficiency, calculated as the Hortonian length (i.e., the inverse of drainage density) divided by the mean unchanneled path length in the tidal flat area (Horton, 1932; Schwarz et al., 2022).

3. Results

3.1. Development process of tidal channel networks

3.1.1. Natural state

Fig. 2a–d portray the spatial characteristics of the channel–flat system simulated in scenario N1, resembling the natural evolution of tidal channel networks. Initially, channels originate from the seaward edge of the computational domain and progressively extend landward (Fig. 2a). Through continuous branching and elongation, a tree-like channel system emerges and intricately dissects the flat, forming a complex channel–flat system. The tidal networks expand rapidly, predominating over the flat within approximately one year. Subsequently, the configuration of the tidal networks stabilizes around the fifth year (Fig. 2b).

Under the influence of continuous sediment input, the tidal flat exhibits a sediment deposition trend. Some secondary creeks gradually recede due to sediment settling, while sediments also accrue along the banks of the primary creeks, leading to gradual narrowing. Simultaneously, the depth of the primary creeks steadily increases owing to the shear stress induced by flow concentration (Fig. 2c and d). Fig. 2e shows the ultimate morphology in scenario N1 at the conclusion of the simulation, characterized by a segmented flat traversed by a tree-like tidal channel system featuring vertical main creeks and horizontal secondary creeks.

3.1.2. Reclamation and de-reclamation state

Fig. 2f–i shows the evolution of tidal networks in scenario C1, which introduces the effects of reclamation and de-reclamation. Similar to the evolution in scenario N1, two trunk creeks quickly develop over the outer area but fail to extend into the reclamation area (Fig. 2f). These trunk creeks penetrate the outer area and gradually give rise to secondary creeks; however, they are obstructed by embankments and unable to extend into the reclamation area (Fig. 2g).

Upon removal of the embankments, channels continue to develop at the ends of the former tidal networks, branch out secondary creeks, and gradually infiltrate the reclamation area (Fig. 2h). While tidal networks in the reclamation area gradually expand, some channels in the outer area recede, as observed in scenario N1 (Fig. 2i). The specific skeleton patterns (central line patterns of the creek system) of the tidal networks exhibit significant disparities between natural conditions and the de-reclamation state. Although intricate tidal channel networks form in the reclamation area in both scenarios, those in scenario C1 are notably less dense. Some main creeks in C1 do not branch out secondary creeks like those in scenario N1, indicating that the tidal channel networks

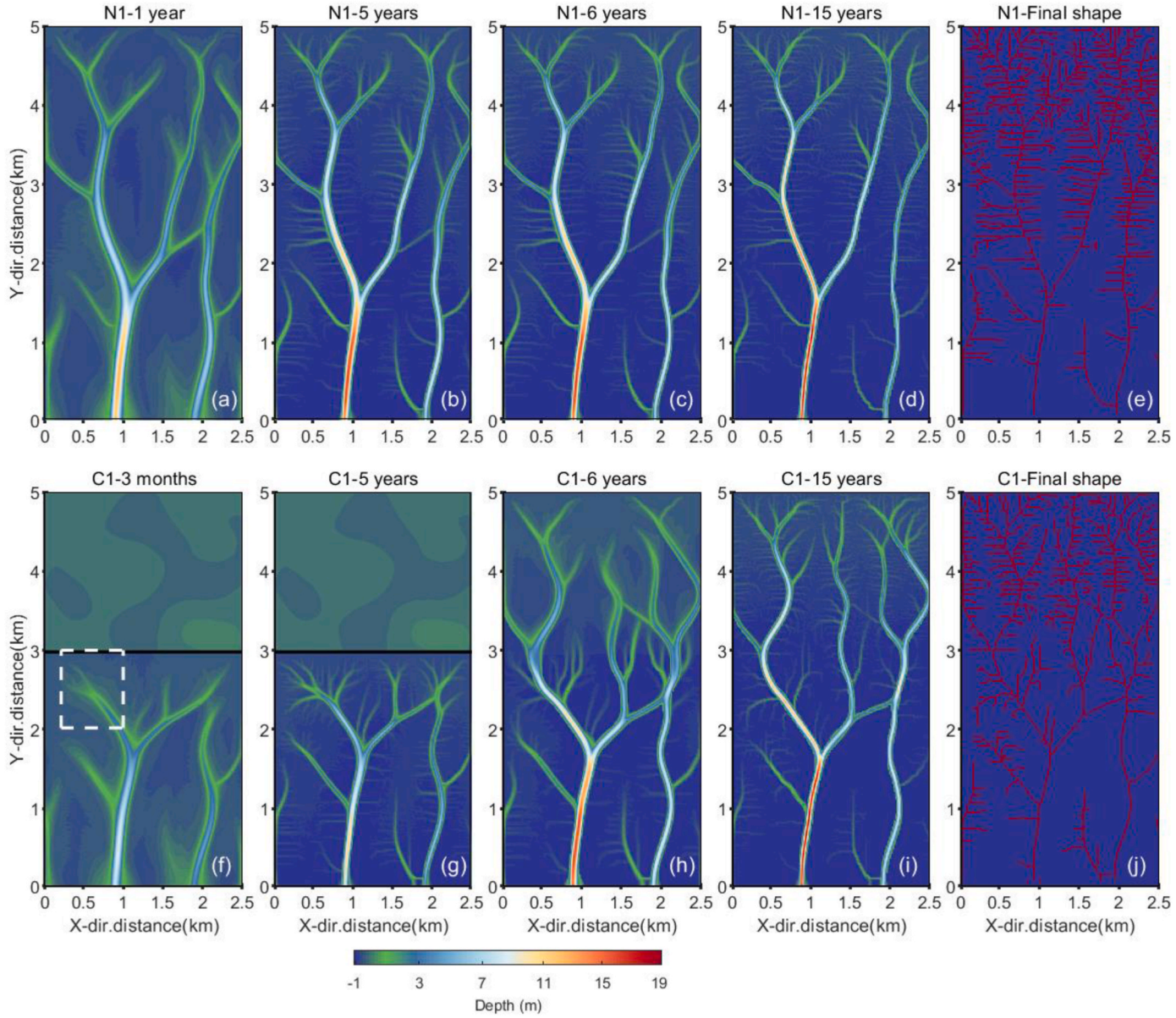

Fig. 2. Morphology evolution in scenarios N1 and C1. (a–d) Morphology evolution under natural state (N1). (f–i) Morphology evolution after reclamation and de-reclamation. Black lines in panels (f) and (g) represent the thin embankments in the first five years, which are removed after de-reclamation. The white dashed square box in panel (g) is a typical area that is analyzed in section 4.2. (e–f) Final skeleton of tidal channel networks in scenarios N1 and C1, respectively.

formed after the de-reclamation project are less developed than those under natural conditions (Fig. 2e and j).

3.2. Morphological evolution trend

Fig. 3a and b illustrate the exceedance probability of the bed elevation in the tidal flat area from the first to the fifteenth year in scenarios N1 and C1. The curve cluster corresponding to the natural state (i.e., scenario N1) progressively increases over time, indicating long-term deposition across the entire tidal flat area (Fig. 3a). In the case of continuous sediment input to the tidal flat and stable tidal network configurations, the elevation of the flat gradually increases. However, this monotonic trend is not observed in scenario C1. The curve cluster in Fig. 3b experiences a sudden drop around the fifth year, coinciding with the de-reclamation project and then increases again.

The 90% cumulative frequency elevation in these two scenarios exhibits a similar difference, with a steady increase in scenario N1 and a sudden decrease around the fifth year, corresponding to the de-reclamation project in scenario C1 (Fig. 3c and d). This suggests that the tidal flat in scenario C1 undergoes brief but significant erosion after de-reclamation, despite continuous sediment input. This erosion is evident during the tidal flat volume change process (Fig. 3e). Both scenarios involve volume losses owing to the rapid expansion of tidal channel networks in the early stages; however, scenario C1 involved additional severe erosion after de-reclamation. This erosion primarily occurs in the outer area, with a volume loss comparable to that observed at the onset of the simulation.

3.3. Tidal network properties

3.3.1. Drainage density

Fig. 4a shows the evolution of the local (i.e., reclamation and outer areas) and overall changes in drainage density in scenarios C1 and N1. For the natural state (i.e., scenario N1), the increase rate of the drainage density of the entire computational domain and outer area begin to decrease after the fourth year. The drainage density of the outer area

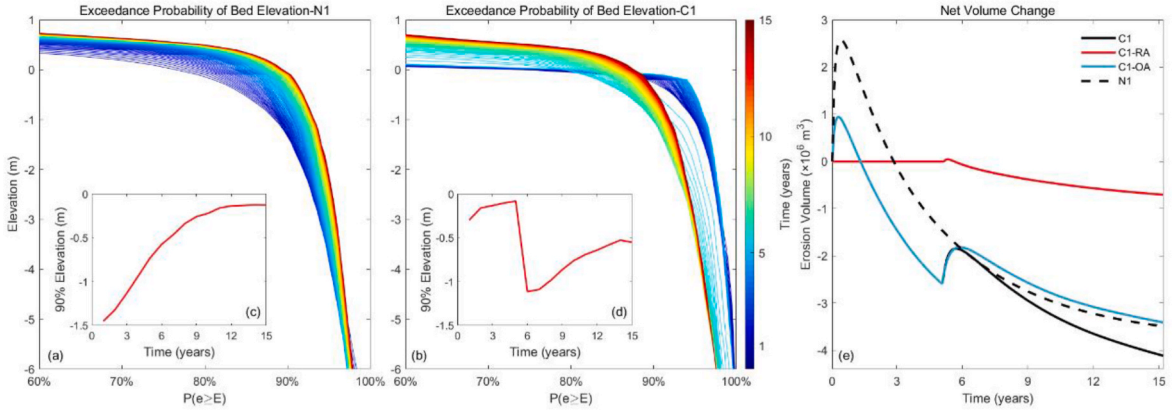

Fig. 3. (A) Exceedance probability distribution of the tidal flat elevation at different times in scenario N1. (b) Exceedance probability of the tidal flat elevation at different times in scenario C1. (c) Changes of the elevation value at 90% cumulative frequency in scenario N1. (d) Change process of the elevation value at 90% cumulative frequency in scenario C1.(e) Net volume change in scenarios C1 and N1. The blue and red solid lines represent the outer and reclamation areas in scenario C1, respectively.

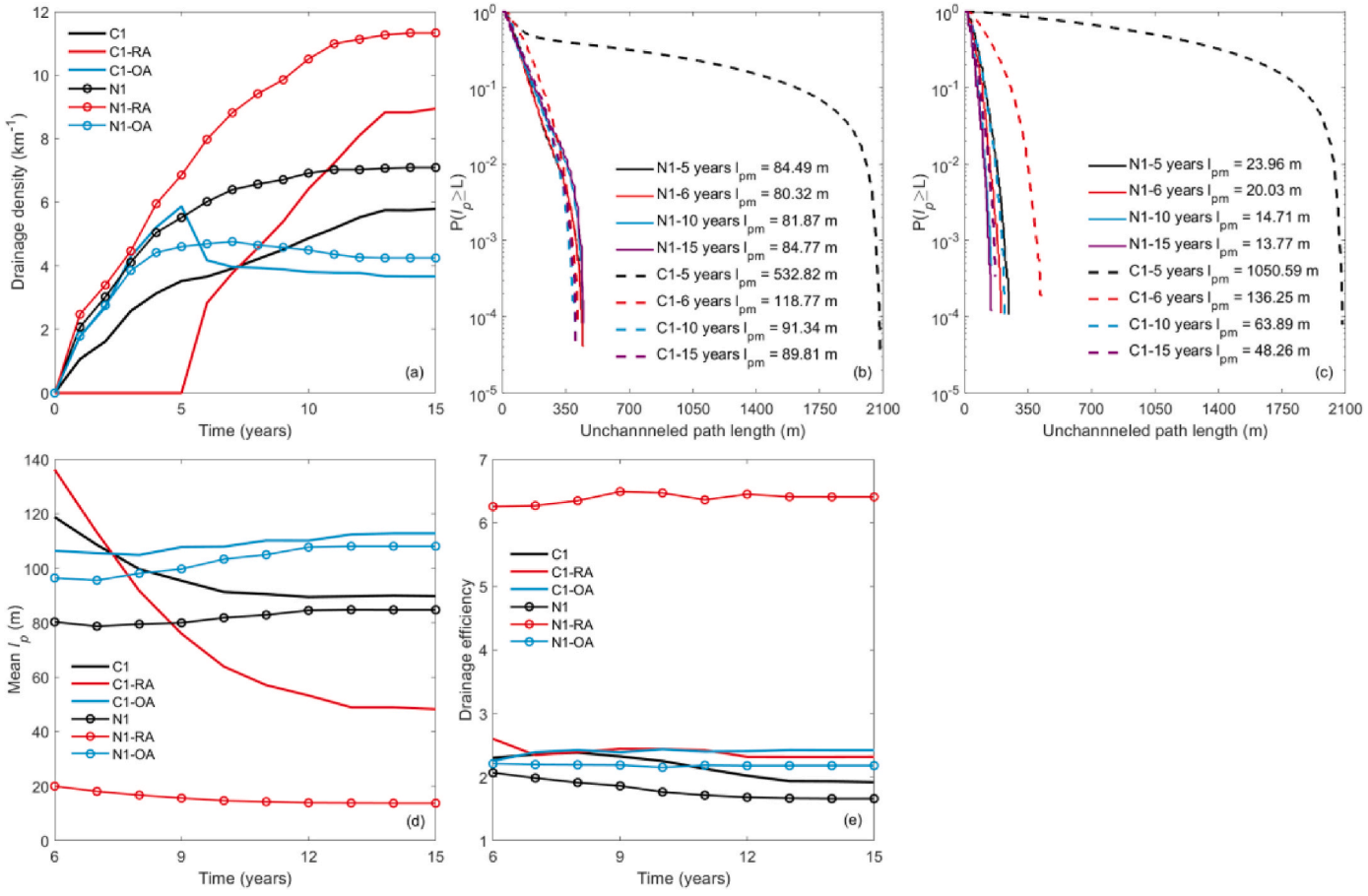

Fig. 4. (A) Drainage density evolution in scenarios C1 and N1. (b) Exceedance probability of the unchanneled path length of the entire flat at different times. (c) Exceedance probability of the unchanneled path length of the reclamation area at different times. (d) Change of l_{pm} after de-reclamation. (e) Drainage efficiency after de-reclamation. Panels (d) and (e) have the same legend.

even slightly decreases after approximately the seventh year, indicating that some channels in the outer area are filled. However, the drainage density in the reclamation area in scenario N1 continuously increases until the eleventh year. This is because the reclamation area is further away from the seaward boundary, and the development process of tidal networks lags behind that in the outer area.

During the reclamation period, channels form only in the outer area. Thus, the drainage density in the outer area in scenario C1 is larger than that in N1; however, the drainage density in the reclamation area remains zero. After the de-reclamation project is implemented, the drainage density in the outer area in scenario C1 rapidly decreases. This is because sediments are eroded and carried downstream after de-reclamation, and some creeks are filled. The final drainage density in the reclamation area in the fifteenth year in scenario C1 is significantly

lower than that in scenario N1. The final drainage density in scenario C1 is 8.95 km^{-1}; in scenario N1, it is 11.33 km^{-1}. In other de-reclamation scenarios with alterations in slope, de-reclamation strategies, and sediment supply, the resulting drainage density similarly falls below that of the natural state (Table 2; a detailed analysis is provided in supplemantary information). Therefore, the de-reclamation project alone cannot fully restore the functions of tidal networks.

3.3.2. Unchanneled path length

Fig. 4b–c display the semilog plots of the exceedance probability of the unchanneled path length ($P \geq l_p$) for the entire tidal flat and reclamation area, respectively, in scenarios C1 and N1. The trends of the curves are approximately linear, which alludes to exponential probability distributions, and therefore, a pointed absence of scale-free properties in the network structures, which is familiar to many field observation results (Belliard et al., 2015; Feola et al., 2005; Marani et al., 2003; Rinaldo et al., 1999). After the fifth year, the network configurations of the natural state remain relatively stable, and both the exceedance probability of the unchanneled path length and the mean value of l_p (l_{pm}) of the flat remain constant (solid lines in Fig. 4b). Regarding the de-reclamation state, the l_{pm} in the fifth year is quite high, because tidal channel networks only exist in the outer area and far from the points in the reclamation area. Dashed lines in Fig. 4b, which represent the exceedance probability of l_p in scenario C1, quickly move to lower left and the l_{pm} values decrease sharply from 532.82 to 118.77 m. Fig. 4c shows specifically the exceedance probability of l_p change in the reclamation area in scenarios N1 and C1 and reveals a similiar process, i.e., the l_{pm} values decrease from 1050.59 to 48.26 m. The change of l_{pm} in the reclamation area in scenarios C1 and N1 from the sixth to the fifteenth year is shown in Fig. 4d. After the de-reclamation project, l_{pm} values in the reclamation area in scenario C1 decrease rapidly, but cannot reach that in scenario N1. At the end of the simulation, the unchanneled path length in scenario C1 is greater than that in scenario N1.

3.3.3. Drainage efficiency

A more thorough description of the capability of the two tidal channel networks in scenarios C1 and N1 can be obtained using the drainage efficiency (Fig. 4e). The e_d values in these two scenarios are almost constant after de-reclamation; however, e_d in the reclamation area in scenario N1 is approximately three times higher than that in scenario C1 (red solid line and red line with circles in Fig. 4e). The e_d values generally depend on the geometry pattern of the tidal channel networks, vegetable cover on tidal flats, and the tidal channel network scale. Higher e_d values in tidal channel networks imply that a larger portion of the marsh platform is close to a channel (Kearney and Fagherazzi, 2016). The l_{pm} values of tidal channel networks with meandering geometries are usually lower than those of tidal channel networks with straight branching geometries, leading to lower e_d values under the same drainage density (Kearney and Fagherazzi, 2016; Schwarz et al., 2022; Schumm and Khan, 1972). The final geometry patterns in scenarios C1 and N1 are both tree-like tidal channel networks and this study did not consider the effects of vegetation. Thus, the main cause of the lower e_d is the tidal channel network scale. Tidal networks generated after de-reclamation are less developed and have lower drainage efficiencies.

Table 2
Final drainage density of scenarios with different slope, de-reclamation strategies, and sediment supply.

Scenario	Drainage density (km^{-1})	Scenario	Drainage density (km^{-1})
C1	8.95	D1	9.07
C2	9.74	D2	10.01
C3	9.39	B1	8.81
S1	10.00	B2	8.38
S2	10.66	B3	7.45
S3	9.97	B4	8.35

4. Discussion

4.1. Effect of landscape settings

The extent of embankment breaching can significantly affect the development and configuration of tidal networks. Residual embankments impede tidal flows and hinder the expansion of tidal networks. Consequently, the total tidal channel length and drainage density in the reclamation area in scenarios B1–B4 are all lower than those in scenario C1. Notably, the final drainage density does not correlate proportionally with the change of the embankment mouth length (l_m). The ultimate drainage density with a smaller mouth length (scenario B1) exceed that with a larger opening (scenario B4). Additionally, when comparing scenarios B2 and B3, the different mouth positions correspond to varying final drainage densities (Table 2).

We calculated the mean unchanneled path length in the reclamation area in scenarios with different de-reclamation strategies in the sixth year, when only main channels are formed. As shown in Fig. 5a, the drainage density of the reclamation area is inversely proportional to l_{pm} during the sixth year. During the development process after de-reclamation, several main channels firstly cut apart the reclamation area and then branches out into secondary channels via headward growth. Owing to the restriction of the remaining embankments, scenarios B2 and B3 form fewer main creeks than those in scenario C1 and lead to a larger unchanneled path length. L_{pm} in C1, B2 and B3 are 135.29 m, 170.93m and 177.32 m, respectively. Similarly, under an equivalent mouth length, the asymmetric opening of the mouth in scenario B3 leads to a higher l_{pm}, resulting in a lower ultimate drainage density compared to that in scenario B2 (Fig. 5b and c).

The scale of the final tidal channel networks is affected by the geographical layout of the main inchoate creeks and l_p at the preliminary stage of the channel development process. This relationship also explains why de-reclamation projects alone cannot fully restore the function of tidal networks. Owing to the restriction of embankments, the tidal channel networks cannot enter the reclamation area in scenario C1. When the embankments are removed, the tidal networks in scenario N1 are much more developed and l_p is much lower. It is difficult for water particles to enter the main channels, and secondary creeks do not easily form through headward erosion under high l_p (Marani et al., 2003; Rinaldo et al., 1999). Thus, the tidal networks in scenario C1 cannot develop to the same scale as those in scenario N1, because scenario C1 starts with fewer main channels and a lower probability of channel headward erosion.

We also applied the de-reclamation project to a tidal channel system exhibiting higher development (scenario P1) and one exhibiting lower development (scenario R1). The morphological characteristics in these two scenarios at the time of de-reclamation implementation can be found in supplemantary information. The eventual drainage density in scenario P1 is higher than that in scenario C1, whereas that in scenario R1 is lower than that in scenario C1 (Fig. 5a). This distinction is also because the more developed tidal channel system in the de-reclamation project has lower l_{pm} and more main creeks, making it easier for secondary channels to form (Fig. 5d and e). This discussion provides suggestions for coastal management. The l_p value at the time when the de-reclamation project primarily occurs can affect the scale that the tidal channel networks can finally reach. The approach adopted in scenario P1 can be regarded as the pre-construction of artificial channels and finally breed out more affluent tidal networks. If the goal is to achieve a more prosperous tidal channel system through de-reclamation projects, it is recommended that certain artificial interventions, such as the construction of artificial channels, be implemented in advance to minimize the unchanneled path length across the flat (Chen et al., 2020; Liu et al., 2020). Several realistic restoration programs have successfully employed the strategic addition of channels to achieve their goals (O'Brien and Zedler, 2006; Liu et al., 2016). Our study contends that this method is not only reliable, but also merits widespread adoption

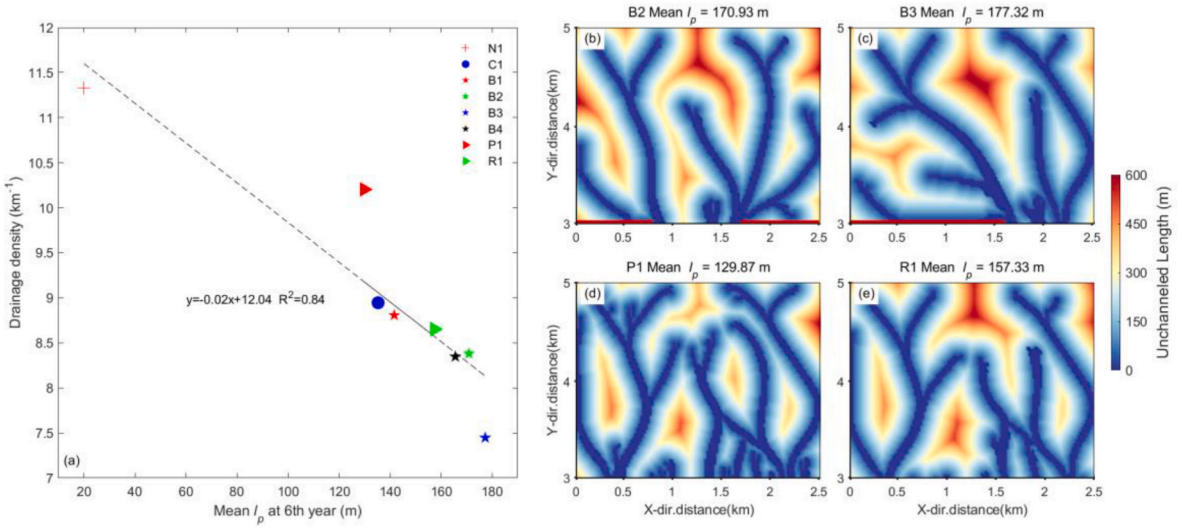

Fig. 5. (A) Correlation graph between the average unchanneled path length at the sixth year and the maximum channel length in the reclamation area. (b–e) Distribution of unchanneled path length in the reclamation area in scenarios B2, B3, P1, and R1, respectively.

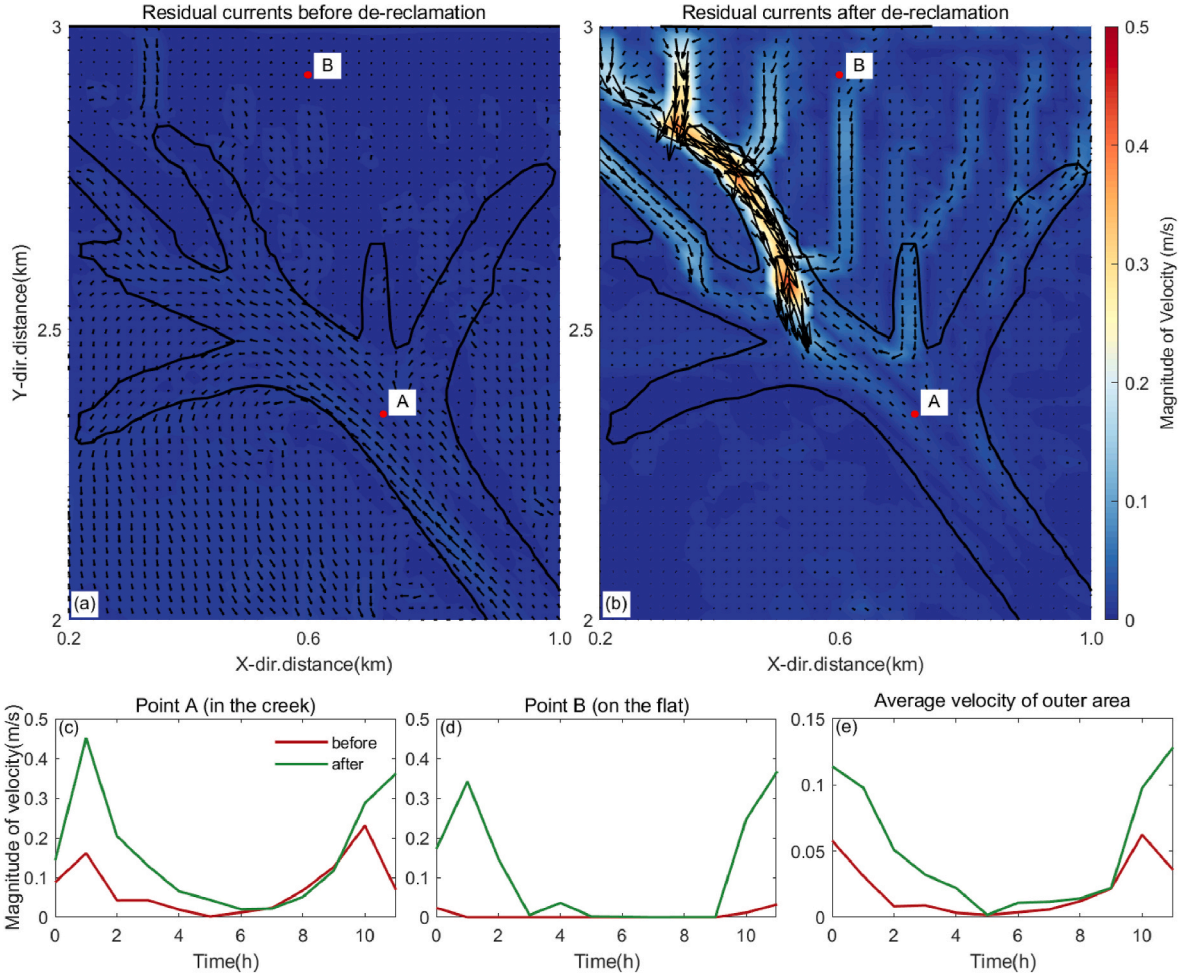

Fig. 6. (A) Residual currents before de-reclamation in the typical area near the embankment toe. The black solid line at the top represents the reclamation embankment. (b) Residual currents after de-reclamation in the typical area. For ease of display, the arrow vectors in panels (a) and (b) indicate only the direction and the color map represents the magnitude in m/s. The black lines in panels (a) and (b) are the 0-m isodeep lines of the typical area. (c) Magnitude of velocity at point A (in the creek). (d) Magnitude of velocity at point B (on the flat). (e) Magnitude of the spatially averaged velocity over the outer area.

because of its proven success in enhancing tidal channel networks.

4.2. Effect of embankment removal

Section 3.2 demonstrates a brief yet intense erosion phase experienced by the tidal flat after de-reclamation (Fig. 3). A typical area with dense creeks near the embankment toe (dashed box in Fig. 2) in the standard scenario C1 is employed as a representative.

Fig. 6a and b compare the residual currents before and after the de-reclamation project by averaging the velocity field over a tidal cycle (Alahmed et al., 2022; Leonardi et al., 2013; Zimmerman, 1981). Before the removal of the embankments, the residual currents in the creeks flow landward, whereas those in the tidal flat area move seaward (Fig. 6a). Owing to the obstruction by the dams, the residual currents near the embankment toe are almost parallel to the embankments. Subsequent removal of the embankments results in changes in both the magnitude and direction of the residual currents (Fig. 6b). The directions of the residual currents in the creeks shift seaward, with the enhancements being even ten-fold. Fig. 6c–e depict the temporal variation of velocity at a point in the creek (Point A), a point on the flat (Point B), and the spatially averaged velocity over the entire outer area and over a tidal cycle. Upon embankment removal, tidal water inundates the reclaimed area, submerging the previously enclosed zone. The tidal prism of the tidal flat undergoes swift augmentation; however, the tidal networks do not expand concomitantly. This suggests that a large volume of tides must be conveyed out of the flat per unit time in the brief period following de-reclamation, resulting in direction turn and a marked increase in velocity.

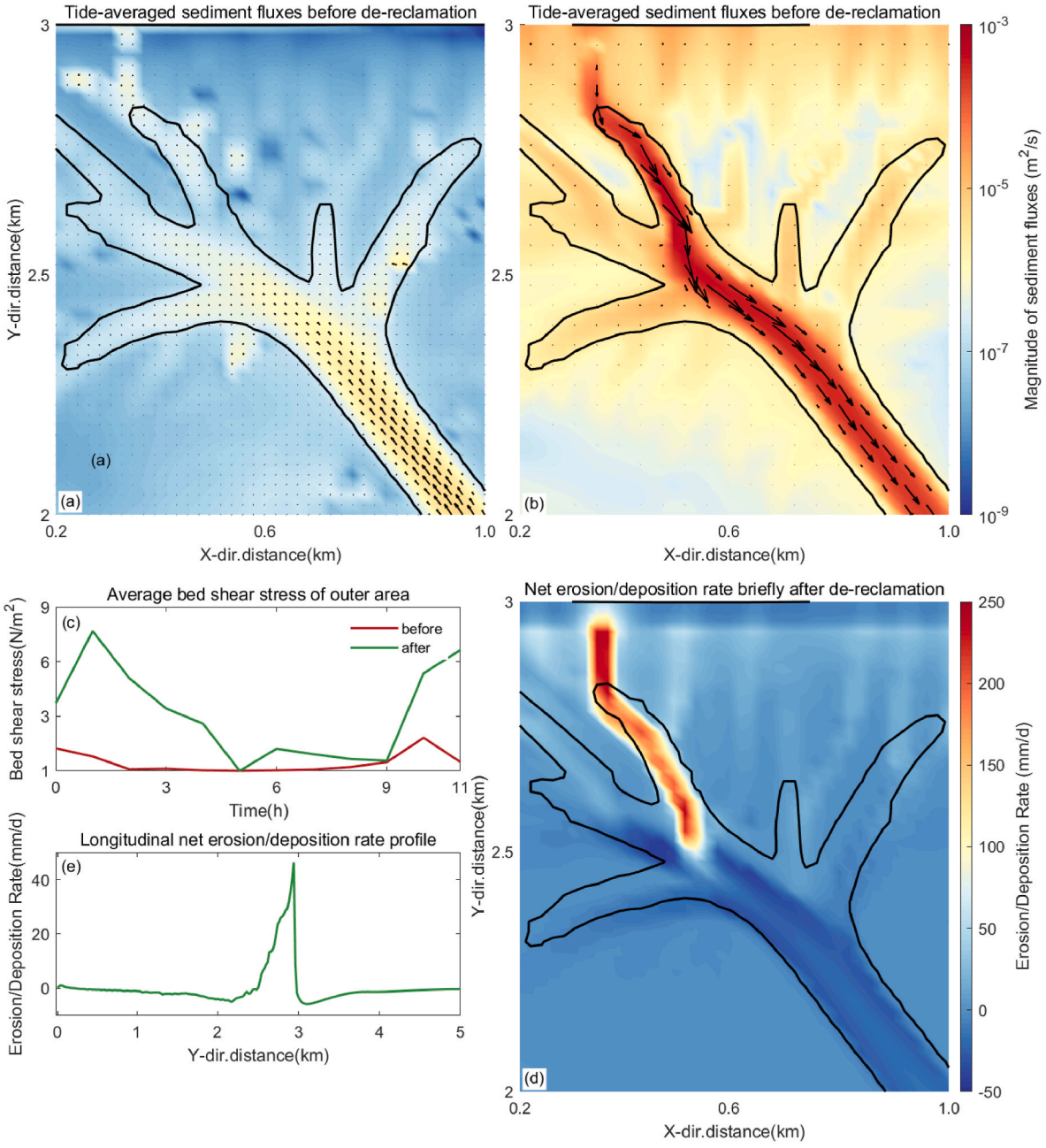

Fig. 7. (A) Tide-averaged sediment fluxes before de-reclamation in the typical area. (b) Tide-averaged sediment fluxes after de-reclamation in the typical area. For ease of display, the arrow vectors in panels (a) and (b) indicate only the direction and the color map represents the magnitude in m^2/s. The black lines in panels (a) and (b) are the 0-m isodeep lines of the typical area. (c) Magnitude of bed shear stress in the outer area before and after de-reclamation over a tidal cycle. (d) Net erosion or deposition rate distribution in the typical area. (e) Net erosion or deposition rate in the five days after de-reclamation on the longitudinal profile.

The enhancement of hydrodynamics in the tidal flat area can significantly magnify the bed shear stresses therein, causing significant sediment erosion and remarkable sediment fluxes (Leonardi et al., 2016; Shi et al., 2012, 2017; Whitehouse et al., 2000). Although strong hydrodynamics have only short durations (such as storms), severe sediment transport can also be caused (Fan et al., 2006; Turner et al., 2006; Xie et al., 2017; Yang et al., 2003). Intense hydrodynamic changes following de-reclamation induce similar effects. Before the de-reclamation project takes place, the tide-averaged sediment fluxes are in the flood direction and of low magnitude, approximately 10^{-9}–10^{-7} m^2/s on the flat and 10^{-6}–10^{-5} m^2/s in the channels, indicating that the tidal flat was laxly deposited under continuous sediment input (Fig. 7a). Similar to the change process of the residual currents, both the direction and magnitude of the sediment fluxes change after de-reclamation. Strong sediment fluxes escape from the channels in the flood direction and the magnitude can be hundred-fold. The tidal flat experiences severe erosion within a short period after de-reclamation (Fig. 7b).

Fig. 7c compares the average magnitude of bed shear stress in the outer area before and after the de-reclamation project over a tidal cycle. Owing to the increased tidal prism and velocity, the bed shear stress of the outer area is significantly enhanced, becoming several times—even dozens of times—higher than that during the reclamation period. Under strong bed shear stress increase and hydrodynamic changes, the tidal flat suffers severe losses. The distribution of the net erosion or deposition rate within a short period (i.e., five days) after de-reclamation is shown in Fig. 7d, the erosion rate at the embankment toe can reach to several tens even hundreds of millimeters per day. The maximum erosion rate is 240.43 mm/d in the typical area. The erosion at the end of the tidal creeks near the embankment toe is the most pronounced. This implies that severe erosion occurs in the form of headward erosion at the tidal channel network edge. After the de-reclamation project, tidal water floods the de-reclamation area and accumulates at the channel tips during the flood period, causing high shear stress and sediment net output.

By analyzing the distribution of net erosion or deposition rate in the five days after de-reclamation on the longitudinal profile, we find that severe erosion is spatially heterogeneous and concentrated near the embankment toe owing to headward erosion at the channel tips (Fig. 7e). The magnitude of severe erosion after de-reclamation can reach more than 1 m locally, many benthic organisms on intertidal flats inhabit this height of tidal flat sediment, and their habitat can be easily affected by sediment erosion (Corte et al., 2017; Hendrick et al., 2016; McCartain et al., 2017; Miller and Sternberg, 1988; Pages et al., 2013). Extreme events with strong hydrodynamic force and severe erosion or deposition, like the severe erosion after de-reclamation, may cause catastrophic losses of these organisms (Hinchey et al., 2006; Thrush et al., 2003). Our study reports severe erosion within a short duration after the de-reclamation project and reveals its potential risks.

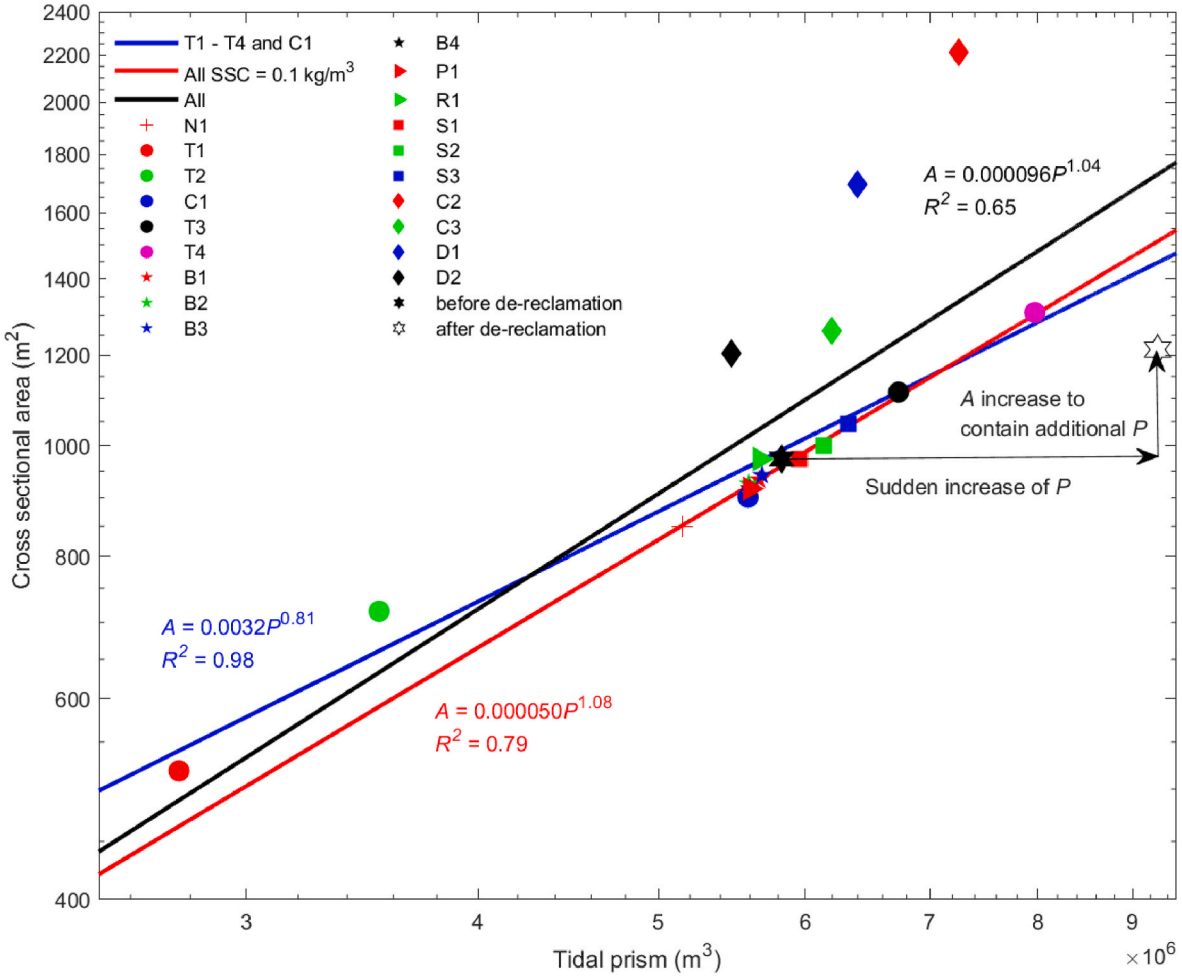

Fig. 8. Sum of the seaward cross-sectional areas plotted as a function of the tidal prism at the end of the simulation. The various markers denote different settings. '+' represents the natural condition. Solid dots represent scenarios T1–T4 and C1, whose tidal amplitudes vary from 0.50 to 1.50 m, separated by 0.25 m. Stars represent the scenarios with embankments partly demolished in different ways. Triangles represent de-reclamation simulations based on different degrees of channel network development. Squares are the scenarios with different slope. Diamonds represent the sediment supply change.

4.3. Evolution of the tidal prism and cross-sectional area

Numerous studies have substantiated the existence of an empirical power law between the tidal prism and the cross-sectional area in tidal inlets or estuaries. This relationship has typically as the following form: $A = kP^n$, where A is the cross-sectional area, P is the tidal prism, and k and n are coefficients determined by the coastal environments that encompass hydrodynamic factors and sediment supply (Geng et al., 2023; D'Alpaos et al., 2009; Hughes, 2002). In this study, the simulated tidal flat is interconnected with the sea via multiple channels; hence, the value of A corresponds to the cumulative seaward cross-sectional area of all channels.

Fig. 8 illustrates the P–A relationships of a series of scenarios upon simulation completion. Scenarios T1–T4 and C1 have identical landscape settings and sediment inputs; however, they differ in tidal amplitude, as indicated by circular dots in Fig. 8. The amplification of the tidal force augments both the tidal prism and the cross-sectional area. The exponent n for this set of scenarios is 0.81, as depicted by the blue line. All final P–A points under the conditions of SSC = 0.1 kg/m^3 and t = 1 m (scenarios N1, C1, B1–B4, P1, and R1) are fitted and shown by the red line. These scenarios maintain uniform hydrodynamic force and sediment input; however, they differ in terms of human influence, with $n = 1.08$. The dispersion of these P–A points is constrained; alterations in landscape settings and the execution of de-reclamation have minor impacts on the P–A relationship. The black line in Fig. 8 represents a fit to all scenarios, incorporating also those with sediment changes (C2, C3, D1, and D2), with $n = 1.04$. The R-square value (0.65) is considerably lower than that of the other fits, indicating that changes in sediment input have a more profound influence on the morphological factors of the tidal flat compared to those of other factors. Therefore, careful consideration of alterations in sediment supply is essential when undertaking de-reclamation projects. The n values obtained from these fits are all in accordance with the range of empirical values (0.80–1.10) cited in existing literature, which is grounded in extensive field observations and theoretical analyses (Hume and Herdendorf, 1993; Jarrett, 1976; O'Brien, 1969). This concordance attests to the fidelity of the numerical experiment designs employed in this study to real-world scenarios.

The movement of hexangular stars in Fig. 8 reports the mechanism of the severe erosion discussed in section 4.2 from the perspective of the P–A relationship. Following the dismantling of the embankments, the tidal prism of the flat experiences significant growth, as indicated by the movement of the black hexagonal star (representing the moment before de-reclamation) to the left. The cross-sectional area should increase homogeneously, mirroring the upward movement of the white hexagonal star (representing the moment after de-reclamation). This adjustment aims to restore the tidal channel system to an equilibrium state, leading to the expansion of channels within a short period following de-reclamation.

P–A points shift towards the top left as the slope of the reclamation area increases, corresponding to the square points in Fig. 8. In the reclamation areas in scenarios S1–S3, the landward-increasing bed surfaces reduce the localized tidal prisms, constraining the expansion of tidal channel networks (Geng et al., 2023). Consequently, more sediment accumulates within the reclamation areas, resulting in a relative reduction of sediment supply to the outer areas (Fig. 9a). Consequently, scenarios S1–S3 differ from scenario C1, and the tidal channels in the outer areas are not extensively filled after de-reclamation; however, they are rather preserved and further expanded with extreme erosion. Eventually, in scenarios S1–S3, the total P and A values within the entire computational domain increase with increasing slope in the reclamation area (Fig. 9b).

4.4. Control factors of severe flat loss

Fig. 10 shows the maximum tidal flat volume loss in the initial two years following de-reclamation under different condition. Over the past 50 years, sediment delivery to estuaries worldwide has declined due to upstream human activities, thereby reducing the sediment supply from estuaries to tidal flats (Cui and Li, 2011; Chen et al., 2005; Syvitski et al., 2005; Zhang et al., 2018; Zhu et al., 2016). Fig. 10a shows the maximum loss volume (V_{lm}) under different constant sediment supply from the estuary. All scenarios experience severe erosion, albeit with different loss volumes inversely related to SSC supply. The maximum loss volume in scenario C1 (SSC = 0.10 kg/m^3) can be four times larger than that in scenario C4 (SSC = 0.25 kg/m^3). When the SSC conditions are similar at the time of de-reclamation, the volume losses are comparable. For instance, both scenarios C1 and D1 have SSC values of 0.10 kg/m^3 in the fifth year, whereas scenarios D3 and D4 have SSC values of 0.30 kg/m^3 (Fig. 10b). The V_{lm} for C1 and D1 are similar, at 7.35×10^5 m^3 and 7.59×10^5 m^3 respectively; similarly, the V_{lm} for D2 and D3 are also close, at 7.64×10^4 m^3 and 7.78×10^4 m^3 respectively. The scenarios presented in Fig. 10c exhibit the same SSC decrease rates; however, their SSC values at the fifth year are different, and the magnitude of V_{lm} is still positively correlated with the in situ SSC at the time of de-reclamation. Severe erosion following de-reclamation is brief yet intense. One of the

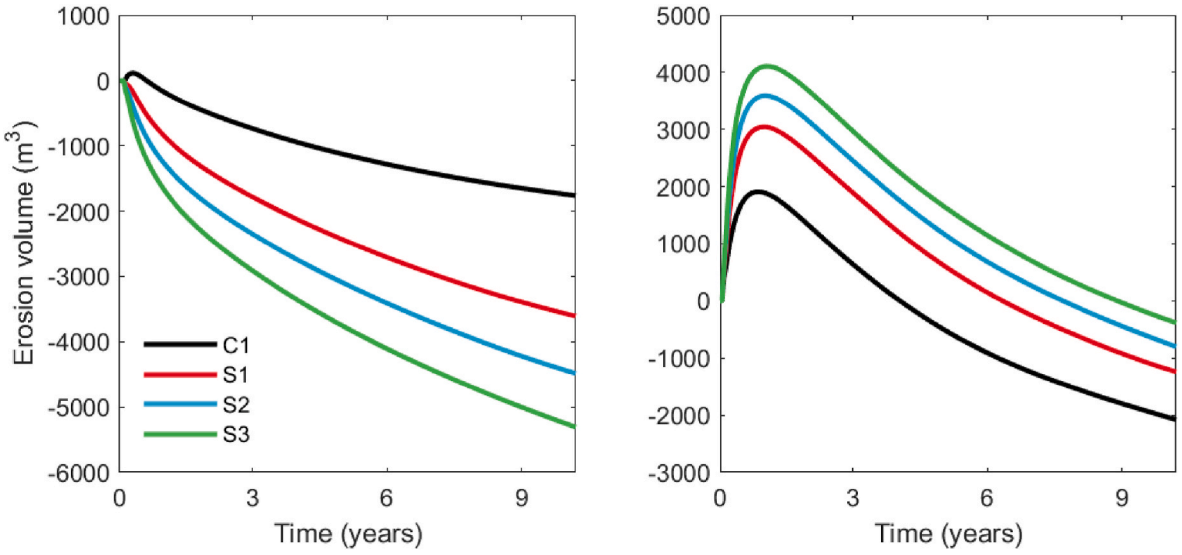

Fig. 9. (A) Erosion volume in the reclamation area in scenarios C1, S1, S2, and S3. (b) Erosion volume in the outer area in scenarios C1, S1, S2, and S3.

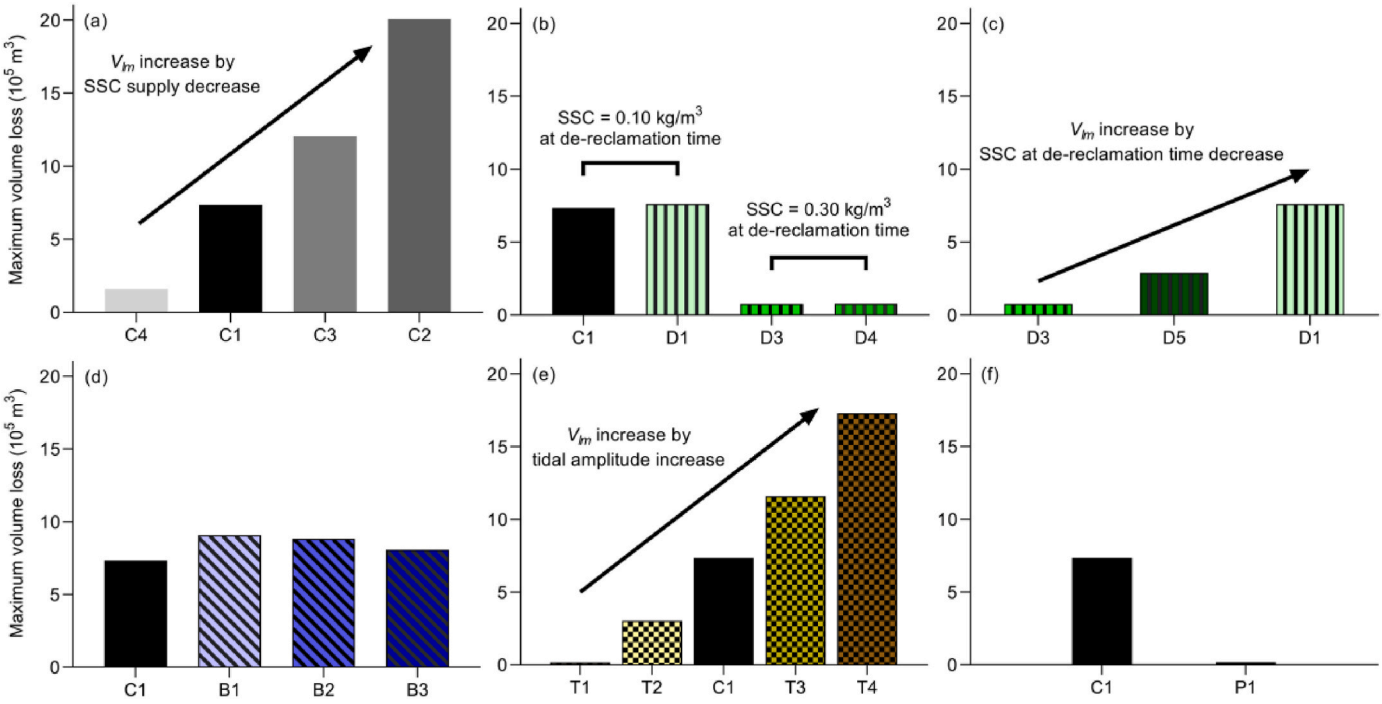

Fig. 10. (A–c) Severe erosion process and flat volume loss under different sediment supply. (d) Severe erosion process under different mode of embankment break. (e) Severe erosion process under different tide condition. (f) Severe erosion process in scenarios C1 and P1.

primary controlling factors of the severe loss is the in situ SSC at the time of de-reclamation; this loss can be reduced in an SSC-abundant environment.

The impacts of landscaping and hydrodynamics on severe loss are illustrated in Fig. 10d and e. Partial demolition of the embankments enhances V_{lm}; conversely, narrower openings can exacerbate severe erosion. Owing to the constraints imposed by the remaining embankments, the flow speed through the open mouth may accelerate, intensifying the shear stress and resulting in a greater volume loss (Fig. 10d). The correlation between the tidal flat volume loss and tidal amplitude is shown in Fig. 10e. Elevated tidal ranges induce higher tidal prisms and augment shear stress, contributing to an increase in V_{lm}. The discrepancy in V_{lm} between scenario B1 ($l_m = 500$ m) and scenario C1 is only 16.79%, and modifications in the de-reclamation methods cannot markedly modulate the severe erosion loss. However, V_{lm} in scenario T4 (1.73×10^6 m^3) is substantially greater—by orders of magnitude—than that in scenario T1 (1.51×10^4 m^3). This indicates that tidal amplitude alterations can significantly influence the severe erosion process. Another pivotal factor controlling the severe erosion volume is the variation of the tidal prism in the tidal flat area.

Fig. 10f shows the volume loss processes in scenarios C1 and P1, with the latter having previously constructed artificial creeks, demonstrating a significant mitigation of severe erosion effects. Pre-constructed channels in the reclamation area can enhance the containment and conveyance capacity of the tidal channel networks at the inception of de-reclamation projects, facilitating accommodation of the abruptly increased tidal prism, and subsequently mitigating the sudden surge in shear stress at the embankment toe. The pre-construction of artificial channels can not only foster tidal channel networks but also diminish the risks associated with severe erosion after de-reclamation. The multifaceted advantages of this approach warrant consideration for engineering applications.

4.5. Recovery following severe tidal flat loss

The net erosion volume change over the entire time period after de-reclamation of the full domain is shown in Fig. 11. Owing to the constant

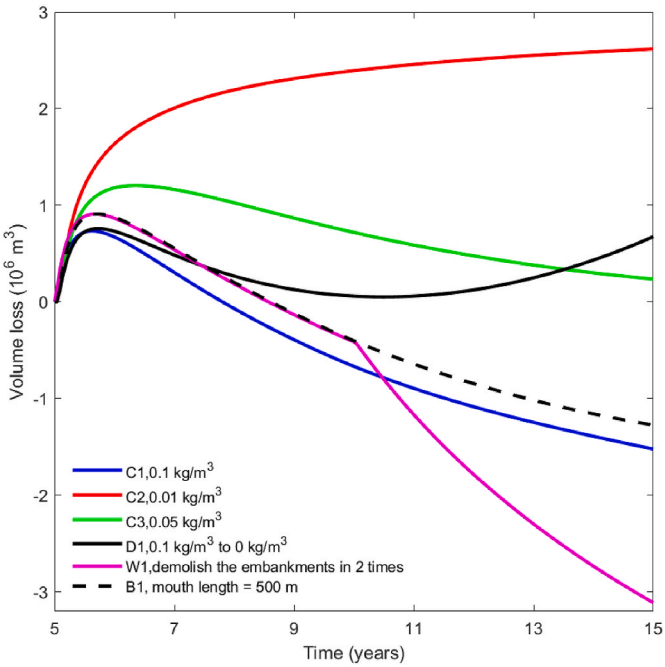

Fig. 11. Net erosion volume change after de-reclamation.

sediment input from the open boundary, the tidal flat is in a state of slow deposition. Although severe erosion occurs after de-reclamation, it can slowly recover under a sufficient and constant sediment supply. For example, the severe erosion in scenario C1 (SSC = 0.1 kg/m^3) basically recovers at around the eighth year (i.e., three years after de-reclamation). Subsequently, the tidal flat continues to exhibit a net deposition trend. However, when the sediment supply is less abundant (scenario C3; SSC = 0.05 kg/m^3), the recovery may take longer. When the sediment supply is very low (scenario C2; SSC = 0.01 kg/m^3), the

severe erosion imprint cannot be recovered.

In scenario D1, where the boundary SSC decrease linearly from 0.10 to 0.00 kg/m^3, the system does not exhibit a changeless depositional trend after the rapid erosional stage; however, it exhibits an erosional tendency after approximately the eleventh year (see the black line in Fig. 11). Note that the averaged SSC boundaries are the same in scenarios C3 and D1; however, in scenario D1, they eventually undergo greater sediment losses. If the sediment supply is insufficient or gradually declines, as in the case of many real estuaries, severe erosion will not be restored and irreversible wetland loss will occur.

The volume change process between the fifth and tenth year (only remove 500 m of embankments) and V_{lm} in scenario W1 are the same as those in scenario B1; however these are not secondary severe erosion after all the embankments are removed. This is because no tidal prism change occurs after the secondary embankment demolition. Removing only part of the embankments can reduce the difficulty and cost of the project but does not mitigate the risk of severe erosion after de-reclamation.

These results imply that short-term severe erosion will become a permanent change when the sediment supply is insufficient, and the decreasing trend in sediment supply can exacerbate the erosion of tidal flats after de-reclamation. Therefore, to offset the negative influences of severe erosion, other coastal management methods can be used jointly, such as practicing sediment nourishment on tidal flats simultaneously with embankment demolition (van der Werf et al., 2015).

4.6. Model limitations

Several processes and factors have either been overlooked or modeled in a simplified manner, as described below:

First, the impact of organisms, including the influence from vegetation and benthic animals, has been neglected. Vegetation can significantly influence the growth of tidal channel networks by affecting soil erodibility, and some channels may extend from bio-created landforms such as crab holes (De Battisti et al., 2019; Geng et al., 2023; Perillo, 2003).

Second, pivotal physical factors such as wind and sea level rise are not incorporated in the design of the numerical experiments. Nevertheless, these elements determine the hydrodynamic forces on the flat and subsequently impact the development of tidal networks (Chen et al., 2008; Ortiz et al., 2017; Coco et al., 2013).

Third, the tidal flat in this study is assumed to be homogeneous, whereas, in reality, significant differences may exist in the physical properties between the reclamation area and the outer area due to human activities (Huang et al., 2021; Wu et al., 2018; Zhang et al., 2018).

Acknowledging these limitations is crucial, as they underline the complexities inherent in real-world tidal flat ecosystems and emphasize the need for further research that incorporates these diverse and interconnected factors to develop more comprehensive and accurate models for predicting the impacts of de-reclamation projects on tidal flats and tidal channel networks.

5. Conclusions

In this study, a state-of-the-art morphodynamic model was adopted to study the development of tidal networks under the combined effects of de-reclamation and decreased sediment supply. We also rivaled and analyzed the potential risk of severe erosion and tidal flat loss after de-reclamation and provided suggestions. Our findings can be summarized as follows.

(1) The final landscape under different settings shows that the restored tidal channel networks have a lower drainage density and efficiency than those of natural ones, and the imprinting of the previous cannot be fully erased simply by de-reclamation.
(2) The ultimate effectiveness of de-reclamation is affected by the geographical layout and unchanneled path length of the inchoate main creek system.
(3) After the embankments are removed, the tidal force is significantly enhanced owing to an increase in the tidal prism contributed by the previously enclosed area. This results in severe tidal flat erosion within a short period.
(4) The extent of severe erosion is related to the tidal prism and sediment supply. If the sediment input is insufficient or gradually declines, the recovery of tidal flats after severe erosion caused by de-reclamation may be irreversible.
(5) Adding artificial channels before de-reclamation projects can promote tidal channel network development and reduce severe erosion after de-reclamation.

CRediT authorship contribution statement

Shang Yu: Conceptualization, Data curation, Formal analysis, Writing – original draft. **Fan Xu:** Conceptualization, Supervision, Writing – review & editing. **Zhong Peng:** Methodology, Software, Writing – review & editing. **Leicheng Guo:** Software, Writing – review & editing. **Xianye Wang:** Data curation, Methodology. **Weiming Xie:** Data curation, Validation. **Chunyan Zhu:** Software. **Zhengbing Wang:** Methodology, Writing – review & editing. **Qing He:** Supervision, Writing – review & editing.

Declaration of competing interest

The authors declare that they have no known competing financial interests or personal relationships that could have appeared to influence the work reported in this paper.

Data availability

Data will be made available on request.

Acknowledgments

This study is financed by Natural Science Foundation of China (NSFC) (Nos. U2040216, 42006150, 42206169, 42276217) and Shanghai Committee of Science and Technology (Nos. 20DZ1204700, 21230750600), and supported by the project ‘Coping with deltas in transition’ within The Programme Strategic Scientific Alliances between China and the Netherlands (PSA).

This article has been partially grammar checked by ChatGPT, an OpenAI language model based in San Francisco, CA, USA.

Appendix A. Supplementary data

Supplementary data to this article can be found online at https://doi.org/10.1016/j.csr.2024.105274.

References

Adam, P., 2002. Saltmarshes in a time of change. Environ. Conserv. 29 (1), 39–61. https://doi.org/10.1017/S0376892902000048.

Alahmed, S., Ross, L., Smith, S.M.C., 2022. Coastal hydrodynamics and timescales in meso-macrotidal estuaries in the gulf of Maine: a model study. Estuar. Coast. https://doi.org/10.1007/s12237-022-01067-9.

Anisfeld, S.C., Hill, T.D., Cahoon, D.R., 2016. Elevation dynamics in a restored versus a submerging salt marsh in long island sound. Estuar. Coast Shelf Sci. 170, 145–154. https://doi.org/10.1016/j.ecss.2016.01.017.

Aronson, J., Le Floc’H, E., 1996. Hierarchies and landscape history: dialoguing with hobbs and norton. Restor. Ecol. 4 (4), 327–333. https://doi.org/10.1111/j.1526-100X.1996.tb00185.x.

Aronson, J., Floret, C., Le Floc’H, E., Ovalle, C., Pontanier, R., 1993. Restoration and rehabilitation of degraded ecosystems in arid and semi-arid lands. II. Case studies in southern Tunisia, Central Chile and northern Cameroon. Restor. Ecol. 1 (3), 168–187. https://doi.org/10.1111/j.1526-100X.1993.tb00023.x.

Belliard, J.P., Toffolon, M., Carniello, L., D'Alpaos, A., 2015. An ecogeomorphic model of tidal channel initiation and elaboration in progressive marsh accretional contexts. J. Geophys. Res.: 120 (6), 1040–1064. https://doi.org/10.1002/2015JF003445.
Cairns, J., Heckman, J.R., 1996. Restoration ecology; the state of an emerging field. Annu. Rev. Energy Environ. 21 (1), 167–189. https://doi.org/10.1146/annurev.energy.21.1.167.
Cadier, C., Bayraktarov, E., Piccolo, R., Adame, M.F., 2020. Indicators of coastal wetlands restoration success: a systematic review. Front. Mar. Sci. 7 https://doi.org/10.3389/fmars.2020.600220.
Chen, C., Qi, J., Li, C., Beardsley, R.C., Lin, H., Walker, R., Gates, K., 2008. Complexity of the flooding/drying process in an estuarine tidal-creek salt-marsh system: an application of FVCOM. J. Geophys. Res. 113 (C7) https://doi.org/10.1029/2007JC004328.
Chen, L., Zhou, Z., Xu, F., Jimenez, M., Tao, J., Zhang, C., 2020. Simulating the impacts of land reclamation and de-reclamation on the morphodynamics of tidal networks. Anthropocene Coasts 3 (1), 30–42. https://doi.org/10.1139/anc-2019-0010.
Chen, X., Zhang, E., Mu, H., Zong, Y., 2005. A preliminary analysis of human impacts on sediment discharges from the yangtze, China, into the sea. J. Coast Res. 213, 515–521. https://doi.org/10.2112/03-0034.1.
Chen, Y., Hsu, W., 1988. A modified fast parallel algorithm for thinning digital patterns. Pattern Recogn. Lett. 7 (2), 99–106. https://doi.org/10.1016/0167-8655(88)90124-9.
Choi, J.Y., Yang, D.B., Hong, G.H., Shin, K.H., 2014. Distribution and bioaccumulation of polychlorinated biphenyls and organochlorine pesticides residues in sediments and Manila clams (Ruditapes philippinarum) from along the Mid-Western coast of Korea. Mar. Pollut. Bull. 85 (2), 672–678. https://doi.org/10.1016/j.marpolbul.2014.05.022.
Choi, Y.R., 2019. Profitable tidal flats, governable fishing communities: assembling tidal flat fisheries in post-crisis South Korea. Polit. Geogr. 72, 20–30. https://doi.org/10.1016/j.polgeo.2019.03.006.
Coco, G., Zhou, Z., van Maanen, B., Olabarrieta, M., Tinoco, R., Townend, I., 2013. Morphodynamics of tidal networks: advances and challenges. Mar. Geol. 346, 1–16. https://doi.org/10.1016/j.margeo.2013.08.005.
Corte, G.N., Schlacher, T.A., Checon, H.H., Barboza, C.A.M., Siegle, E., Coelman, R.A., Amaral, A.C.Z., 2017. Storm effects on intertidal invertebrates: increased beta diversity of few individuals and species. PeerJ 5, e3360.
Cui, B., Li, X., 2011. Coastline change of the Yellow River estuary and its response to the sediment and runoff (1976–2005). Geomorphology 127 (1–2), 32–40. https://doi.org/10.1016/j.geomorph.2010.12.001.
D'Alpaos, A., Lanzoni, S., Marani, M., Bonometto, A., Cecconi, G., Rinaldo, A., 2007. Spontaneous tidal network formation within a constructed salt marsh: observations and morphodynamic modelling. Geomorphology 91 (3–4), 186–197. https://doi.org/10.1016/j.geomorph.2007.04.013.
D'Alpaos, A., Lanzoni, S., Marani, M., Rinaldo, A., 2009. On the O'Brien-Jarrett-Marchi law. Rendiconti Lincei 20 (3), 225–236. https://doi.org/10.1007/s12210-009-0052-x.
De Battisti, D., Fowler, M.S., Jenkins, S.R., Skov, M.W., Rossi, M., Bouma, T.J., Neyland, P.J., Griffin, J.N., 2019. Intraspecific root trait variability along environmental gradients affects salt marsh resistance to lateral erosion. Frontiers in Ecology and Evolution 7. https://doi.org/10.3389/fevo.2019.00150.
Desroy, N., Denis, L., 2004. Influence of spring phytodetritus sedimentation on intertidal macrozoobenthos in the eastern English Channel. Marine Ecology Progress 270 (Apr), 41–53. https://doi.org/10.3354/meps270041.
Duarte, C.M., Dennison, W.C., Orth, R.J.W., Carruthers, T.J.B., 2008. The charisma of coastal ecosystems: addressing the imbalance. Estuar. Coast 31 (2), 233–238. https://doi.org/10.1007/s12237-008-9038-7.
Fagherazzi, S., Bortoluzzi, A., Dietrich, W.E., Adami, A., Lanzoni, S., Marani, M., Rinaldo, A., 1999. Tidal networks; 1, automatic network extraction and preliminary scaling features from digital terrain maps. Water Resour. Res. 35 (12), 3891–3904. https://doi.org/10.1029/1999WR900236.
Fagherazzi, S., Kirwan, M.L., Mudd, S.M., Guntenspergen, G.R., Temmerman, S., D'Alpaos, A., van de Koppel, J., Rybczyk, J.M., Reyes, E., Craft, C., Clough, J., 2012. Numerical models of salt marsh evolution: ecological, geomorphic, and climatic factors. Rev. Geophys. 50 (1) https://doi.org/10.1029/2011RG000359.
Fan, D., Guo, Y., Wang, P., Shi, J.Z., 2006. Cross-shore variations in morphodynamic processes of an open-coast mudflat in the Changjiang Delta, China: with an emphasis on storm impacts. Continent. Shelf Res. 26 (4), 517–538. https://doi.org/10.1016/j.csr.2005.12.011.
Feola, A., Belluco, E., D'Alpaos, A., Lanzoni, S., Marani, M., Rinaldo, A., 2005. A geomorphic study of lagoonal landforms. Water Resour. Res. 41 (6) https://doi.org/10.1029/2004WR003811.
French, P.W., 1999. Managed retreat: a natural analogue from the medway estuary, UK. Ocean Coast Manag. 42 (1), 49–62. https://doi.org/10.1016/S0964-5691(98)00079-9.
Geng, L., Lanzoni, S., D'Alpaos, A., Sgarabotto, A., Gong, Z., 2023. The sensitivity of tidal channel systems to initial bed conditions, vegetation, and tidal asymmetry. J. Geophys. Res.: Earth Surf. 128 (3) https://doi.org/10.1029/2022JF006929.
Goudie, A., 2013. Characterising the distribution and morphology of creeks and pans on salt marshes in England and Wales using Google Earth. Estuar. Coast Shelf Sci. 129, 112–123. https://doi.org/10.1016/j.ecss.2013.05.015.
Gu, J., Luo, M., Zhang, X., Christakos, G., Agusti, S., Duarte, C.M., Wu, J., 2018. Losses of salt marsh in China: trends, threats and management. Estuar. Coast Shelf Sci. 214, 98–109. https://doi.org/10.1016/j.ecss.2018.09.015.
Guo, L., van der Wegen, M., Roelvink, D.J.A., Wang, Z.B., He, Q., 2015. Long-term, process-based morphodynamic modeling of a fluvio-deltaic system, Part I: the role of river discharge. Continent. Shelf Res. 109, 95–111. https://doi.org/10.1016/j.csr.2015.09.002.
Hendrick, V.J., Hutchison, Z.L., Last, K.S., 2016. Sediment burial intolerance of marine macroinvertebrates. PLoS One 11 (2), e0149114. https://doi.org/10.1371/journal.pone.0149114.
Hinchey, E.K., Schaffner, L.C., Hoar, C.C., Vogt, B.W., Batte, L.P., 2006. Responses of estuarine benthic invertebrates to sediment burial: the importance of mobility and adaptation. Hydrobiologia 556 (1), 85–98. https://doi.org/10.1007/s10750-005-1029-0.
Horton, R.E., 1932. Drainage-basin characteristics. Eos, Transactions American Geophysical Union 13. https://doi.org/10.1029/TR013i001p00350.
Hu, K., Ding, P., Wang, Z., Yang, S., 2009. A 2D/3D hydrodynamic and sediment transport model for the yangtze estuary, China. J. Mar. Syst. 77 (1–2), 114–136. https://doi.org/10.1016/j.jmarsys.2008.11.014.
Hughes, S.A., 2002. Equilibrium cross sectional area at tidal inlets. J. Coast Res. 18, 160–174. ISSN 0749-0208. https://api.semanticscholar.org/CorpusID:54678398.
Hume, T.M., Herdendorf, C.E., 1993. On the use of empirical stability relationships for characterizing estuaries. J. Coast Res. 9, 413–422. https://www.jstor.org/stable/4298099.
Jarzemsky, R.D., Burchell, M.R., Evans, R.O., 2013. The impact of manipulating surface topography on the hydrologic restoration of a forested coastal wetland. Ecol. Eng. 58, 35–43. https://doi.org/10.1016/j.ecoleng.2013.06.002.
Jarrett, J.T., 1976. Tidal Prism-Inlet Area Relationships. https://usace.contentdm.oclc.org/digital/api/collection/p266001coll1/id/7466/.
Katwijk, M.M.V., Thorhaug, A., Marba, N., Orth, R.J., Duarte, C.M., Kenick, G.A., Althuizen, I.H.J., Balestri, E., Bernard, G., Cambridge, M.L., Cunha, A., Durance, C., Giesen, W., Han, Q.Y., Hosokawa, S., Kiswara, W., Komatsu, T., Lardicci, C., Lee, K.S., Meinesz, A., Nakaoka, M., O'Brien, K.R., Paling, E.I., Pickerell, C., Ransijn, A.M.A., Verduin, J.J., Österblom, H., 2016. Global analysis of seagrass restoration: the importance of large-scale planting. J. Appl. Ecol. 53 (2), 567–578. https://doi.org/10.1111/1365-2664.12562.
Kearney, W.S., Fagherazzi, S., 2016. Salt marsh vegetation promotes efficient tidal channel networks. Nat. Commun. 7 (1) https://doi.org/10.1038/ncomms12287.
Lee, J., Chung, O., Park, J., Kim, H., Hur, W., Kim, S., Kim, J., 2018. Effects of the saemangeum reclamation project on migratory shorebird staging in the saemangeum and geum estuaries, South Korea. Bird. Conserv. Int. 28 (2), 238–250. https://doi.org/10.1017/S0959270916000605.
Leonard, L.A., Hine, A.C., Luther, M.E., Stumpf, R.P., Wright, E.E., 1995. Sediment transport processes in a west-central Florida open marine marsh tidal creek; the role of tides and extra-tropical storms. Estuar. Coast Shelf Sci. 41 (2), 225–248. https://doi.org/10.1006/ecss.1995.0063.
Leonardi, N., Canestrelli, A., Sun, T., Fagherazzi, S., 2013. Effect of tides on mouth bar morphology and hydrodynamics. J. Geophys. Res.: Oceans 118 (9), 4169–4183. https://doi.org/10.1002/jgrc.20302.
Leonardi, N., Ganju, N.K., Fagherazzi, S., 2016. A linear relationship between wave power and erosion determines salt-marsh resilience to violent storms and hurricanes. Proc. Natl. Acad. Sci. USA 113 (1), 64–68. https://doi.org/10.1073/pnas.1510095112.
Lesser, G.R., Roelvink, J.A., van Kester, J.A.T.M., Stelling, G.S., 2004. Development and validation of a three-dimensional morphological model. Coastal Engineering 51 (8–9), 883–915. https://doi.org/10.1016/j.coastaleng.2004.07.014.
Liu, Z., Cui, B., He, Q., 2016. Shifting paradigms in coastal restoration: six decades' lessons from China. Sci. Total Environ. 566–567, 205–214. https://doi.org/10.1016/j.scitotenv.2016.05.049.
Liu, Z., Fagherazzi, S., She, X., Ma, X., Xie, C., Cui, B., 2020. Efficient tidal channel networks alleviate the drought-induced die-off of salt marshes: implications for coastal restoration and management. Sci. Total Environ. 749, 141493 https://doi.org/10.1016/j.scitotenv.2020.141493.
Liu, Z., Fagherazzi, S., Cui, B., 2021. Success of coastal wetlands restoration is driven by sediment availability. Communications Earth & Environment 2 (1). https://doi.org/10.1038/s43247-021-00117-7.
Marciano, R., 2005. Modeling of channel patterns in short tidal basins. J. Geophys. Res. 110 (F1) https://doi.org/10.1029/2003JF000092.
Marani, M., Lanzoni, S., Zandolin, D., Seminara, G., Rinaldo, A., 2002. Tidal meanders. Water Resour. Res. 38 (11) https://doi.org/10.1029/2001WR000404.
Marani, M., Belluco, E., D'Alpaos, A., Defina, A., Lanzoni, S., Rinaldo, A., 2003. On the drainage density of tidal networks. Water Resour. Res. 39 (2) https://doi.org/10.1029/2001WR001051.
McCartain, L.D., Townsend, M., Thrush, S.F., Wethey, D.S., Woodin, S.A., Volkenborn, N., Pilditch, C.A., 2017. The effects of thin mud deposits on the behaviour of a deposit-feeding tellinid bivalve: implications for ecosystem functioning. Mar. Freshw. Behav. Physiol. 50 (4), 239–255. https://doi.org/10.1080/10236244.2017.1364123.
Miller, D.C., Sternberg, R.W., 1988. Field measurements of the fluid and sediment-dynamic environment of a benthic deposit feeder. J. Mar. Res. 46 (4), 771–796. https://elischolar.library.yale.edu/journal_of_marine_research/1912.
Mumby, P., Steneck, R., 2008. Coral reef management and conservation in light of rapidly evolving ecological paradigms. Trends Ecol. Evol. 23 (10), 555–563. https://doi.org/10.1016/j.tree.2008.06.011.
Murray, N.J., Phinn, S.R., DeWitt, M., Ferrari, R., Johnston, R., Lyons, M.B., Clinton, N., Thau, D., Fuller, R.A., 2019. The global distribution and trajectory of tidal flats. Nature 565 (7738), 222–225. https://doi.org/10.1038/s41586-018-0805-8.
O'Brien, M.P., 1969. Equilibrium flow areas of inlets on sandy coasts. J. Waterw. Harb. Div. 95 (1), 43–52. https://doi.org/10.1061/JWHEAU.0000622.

Ortiz, A.C., Roy, S., Edmonds, D.A., 2017. Land loss by pond expansion on the Mississippi River delta plain. Geophys. Res. Lett. 44 (8), 3635–3642. https://doi.org/10.1002/2017GL073079.

Pages, J.F., Gera, A., Romero, J., Farina, S., Garcia-Rubies, A., Hereu, B., Alcoverro, T., 2013. The mediterranean benthic herbivores show diverse responses to extreme storm disturbances. PLoS One 8 (5), e62719. https://doi.org/10.1371/journal.pone.0062719.

Pendleton, L., et al., 2012. Estimating global "blue carbon" emissions from conversion and degradation of vegetated coastal ecosystems. PLoS One 7 (9), e43542. https://doi.org/10.1371/journal.pone.0043542.

Perillo, G.M.E., 2003. New mechanisms studied for creek formation in tidal flats; from crabs to tidal channels. American Geophysical Union 1–5. https://doi.org/10.1029/2003EO010001. Washington, DC.

Rauch, M., Denis, L., 2008. Spatio-temporal variability in benthic mineralization processes in the eastern English Channel. Biogeochemistry 89 (2), 163–180. https://doi.org/10.1007/s10533-008-9191-x.

Ren, H., Wu, X., Ning, T., Huang, G., Wang, J., Jian, S., Lu, H., 2011. Wetland changes and mangrove restoration planning in shenzhen bay, southern China. Landsc. Ecol. Eng. 7 (2), 241–250. https://doi.org/10.1007/s11355-010-0126-z.

Rinaldo, A., Fagherazzi, S., Lanzoni, S., Marani, M., Dietrich, W.E., 1999. Tidal networks: 2. Watershed delineation and comparative network morphology. Water Resour. Res. 35 (12), 3905–3917. https://doi.org/10.1029/1999WR900237.

Saxena, L.P., 2019. Niblack's binarization method and its modifications to real-time applications: a review. Artif. Intell. Rev. 51 (4), 673–705. https://doi.org/10.1007/s10462-017-9574-2.

Schumm, S.A., Khan, H.R., 1972. Experimental study of channel patterns. Nature 233, 407–409. https://doi.org/10.1038/233407a0, 1971.

Schwarz, C., van Rees, F., Xie, D., Kleinhans, M.G., van Maanen, B., 2022. Salt marshes create more extensive channel networks than mangroves. Nat. Commun. 13 (1) https://doi.org/10.1038/s41467-022-29654-1.

Shi, B.W., Yang, S.L., Wang, Y.P., Li, G.C., Li, M.L., Li, P., Li, C., 2017. Role of wind in erosion-accretion cycles on an estuarine mudflat. J. Geophys. Res.: Oceans 122 (1), 193–206. https://doi.org/10.1002/2016JC011902.

Shi, B.W., Yang, S.L., Wang, Y.P., Bouma, T.J., Zhu, Q., 2012. Relating accretion and erosion at an exposed tidal wetland to the bottom shear stress of combined current–wave action. Geomorphology 138 (1), 380–389. https://doi.org/10.1016/j.geomorph.2011.10.004.

Simenstad, C., Reed, D., Ford, M., 2006. When is restoration not? Ecol. Eng. 26 (1), 27–39. https://doi.org/10.1016/j.ecoleng.2005.09.007.

Stefanon, L., Carniello, L., D'Alpaos, A., Rinaldo, A., 2012. Signatures of sea level changes on tidal geomorphology: experiments on network incision and retreat. Geophys. Res. Lett. 39 (12) https://doi.org/10.1029/2012GL051953.

Susanne, R., Robert, J.N., 2007. Coastal and estuarine retreat: a comparison of the application of managed realignment in england and Germany. J. Coast Res. 2007 (236), 1418–1430. https://doi.org/10.2112/04-0426.1.

Syvitski, J.P.M., Vorosmarty, C.J., Kettner, A.J., Green, P., 2005. Impact of humans on the flux of terrestrial sediment to the global coastal ocean. Science (American Association for the Advancement of Science) 308 (5720), 376–380. https://doi.org/10.1126/science.1109454.

Takekawa, J.Y., Woo, I., Athearn, N.D., Demers, S., Gardiner, R.J., Perry, W.M., Ganju, N. K., Shellenbarger, G.G., Schoellhamer, D.H., 2010. Measuring sediment accretion in early tidal marsh restoration. Wetl. Ecol. Manag. 18 (3), 297–305. https://doi.org/10.1007/s11273-009-9170-6.

Thrush, S.F., Hewitt, J.E., Norkko, A., Cummings, V.J., Funnell, G.A., 2003. Macrobenthic recovery processes following catastrophic sedimentation on estuarine sandflats. Ecol. Appl. 13 (5), 1433–1455. https://doi.org/10.1890/02-5198.

Turner, R.E., Baustian, J.J., Swenson, E.M., Spicer, J.S., 2006. Wetland sedimentation from hurricanes katrina and rita. Science (American Association for the Advancement of Science) 314 (5798), 449–452. https://doi.org/10.1126/science.1129116.

Uchida, S., 2013. Image processing and recognition for biological images. Dev. Growth Differ. 55 (4), 523–549. https://doi.org/10.1111/dgd.12054.

van der Wegen, M., Roelvink, J.A., 2008. Long-term morphodynamic evolution of a tidal embayment using a two-dimensional, process-based model. J. Geophys. Res. 113 (C3) https://doi.org/10.1029/2006JC003983.

van der Wegen, M., Roelvink, J.A., 2012. Reproduction of estuarine bathymetry by means of a process-based model: western Scheldt case study, The Netherlands. Geomorphology 179, 152–167. https://doi.org/10.1016/j.geomorph.2012.08.007.

van der Werf, J., Reinders, J., van Rooijen, A., Holzhauer, H., Ysebaert, T., 2015. Evaluation of a tidal flat sediment nourishment as estuarine management measure. Ocean Coast Manag. 114, 77–87. https://doi.org/10.1016/j.ocecoaman.2015.06.006.

Wang, Y., Wang, Y.P., Yu, Q., Du, Z., Wang, Z.B., Gao, S., 2019. Sand-mud tidal flat morphodynamics influenced by alongshore tidal currents. J. Geophys. Res.: Oceans 124 (6), 3818–3836. https://doi.org/10.1029/2018JC014550.

Whitehouse, R.J.S., Bassoullet, P., Dyer, K.R., Mitchener, H.J., Roberts, W., Dyer, K.R., 2000. The influence of bedforms on flow and sediment transport over intertidal mudflats. Continent. Shelf Res. 20 (10–11), 1099–1124. https://doi.org/10.1016/S0278-4343(00)00014-5.

Wiberg, P.L., Carr, J.A., Safak, I., Anutaliya, A., 2015. Quantifying the distribution and influence of non-uniform bed properties in shallow coastal bays. Limnol Oceanogr. Methods 13 (12), 746–762. https://doi.org/10.1002/lom3.10063.

Williams, P.B., Orr, M.K., Garrity, N.J., 2002. Hydraulic geometry: a geomorphic design tool for tidal marsh channel evolution in wetland restoration projects. Restor. Ecol. 10 (3), 577–590. https://doi.org/10.1046/j.1526-100X.2002.t01-1-02035.x.

Wolters, M., Garbutt, A., Bakker, J.P., 2005. Salt-marsh restoration: evaluating the success of de-embankments in north-west europe. Biol. Conserv. 123 (2), 249–268. https://doi.org/10.1016/j.biocon.2004.11.013.

Wu, W., Yang, Z., Tian, B., Huang, Y., Zhou, Y., Zhang, T., 2018. Impacts of coastal reclamation on wetlands: loss, resilience, and sustainable management. Estuar. Coast Shelf Sci. 210, 153–161. https://doi.org/10.1016/j.ecss.2018.06.013.

Xie, W., He, Q., Zhang, K., Guo, L., Wang, X., Shen, J., Cui, Z., 2017. Application of terrestrial laser scanner on tidal flat morphology at a typhoon event timescale. Geomorphology 292, 47–58. https://doi.org/10.1016/j.geomorph.2017.04.034.

Xie, W., He, Q., Wang, X., Guo, L., Zhang, K., 2018. Role of mudflat-creek sediment exchanges in intertidal sedimentary processes. J. Hydrol. 567, 351–360. https://doi.org/10.1016/j.jhydrol.2018.10.027.

Xu, F., Coco, G., Zhou, Z., Tao, J., Zhang, C., 2017. A numerical study of equilibrium states in tidal network morphodynamics. Ocean Dynam. 67 (12), 1593–1607. https://doi.org/10.1007/s10236-017-1101-0.

Yang, H., Chen, B., Barter, M., Piersma, T., Zhou, C., Li, F., Zhang, Z., 2011. Impacts of tidal land reclamation in bohai bay, China: ongoing losses of critical yellow sea waterbird staging and wintering sites. Bird. Conserv. Int. 21 (3), 241–259. https://doi.org/10.1017/S0959270911000086.

Yang, S., Friedrichs, C.T., Shi, Z., Ding, P., Zhu, J., Zhao, Q., 2003. Morphological response of tidal marshes, flats and channels of the outer yangtze river mouth to a major storm. Estuaries 26 (6), 1416–1425. https://doi.org/10.1007/BF02803650.

Yang, Z., Khangaonkar, T., Calvi, M., Nelson, K., 2010. Simulation of cumulative effects of nearshore restoration projects on estuarine hydrodynamics. Ecol. Model. 221 (7), 969–977.

Zhang, Y., Zhou, Z., Geng, L., Coco, G., Tao, J., Zhang, C., 2018. Simulating the formation of tidal channels along an open-coast tidal flat: the effects of initial perturbation. Coastal Engineering Proceedings 1, 84. https://doi.org/10.1016/j.gloplacha.2004.01.008.

Zhong, Z., Hu, Z., 2021. The impact of reclamation on tidal flat morphological equilibrium. Front. Mar. Sci. 8 https://doi.org/10.3389/fmars.2021.769077.

Zhou, Z., Coco, G., Jiménez, M., Olabarrieta, M., van der Wegen, M., Townend, I., 2014. Morphodynamics of river-influenced back-barrier tidal basins: the role of landscape and hydrodynamic settings. Water Resour. Res. 50 (12), 9514–9535. https://doi.org/10.1002/2014WR015891.

Zhou, Z., Liu, Q., Fan, D., Coco, G., Gong, Z., Möller, I., Xu, F., Townend, I., Zhang, C., 2021. Simulating the role of tides and sediment characteristics on tidal flat sorting and bedding dynamics. Earth Surf. Process. Landforms 46 (11), 2163–2176. https://doi.org/10.1002/esp.5166.

Zhu, L., He, Q., Shen, J., Wang, Y., 2016. The influence of human activities on morphodynamics and alteration of sediment source and sink in the Changjiang Estuary. Geomorphology 273, 52–62. https://doi.org/10.1016/j.geomorph.2016.07.025.

Zimmerman, J.T.F., 1981. Dynamics, diffusion and geomorphological significance of tidal residual eddies. Nature (London) 290 (5807), 549–555. https://doi.org/10.1038/290549a0.